Research Article

NMR IN BIOMEDICINE

Received: 17 August 2010, Revised: 20 May 2011, Accepted: 20 May 2011, Published online in Wiley Online Library: 2011

(wileyonlinelibrary.com) DOI: 10.1002/nbm.1765

Multimodal assessment of early tumor response to chemotherapy: comparison between diffusion-weighted MRI, ^{1}H-MR spectroscopy of choline and USPIO particles targeted at cell death

K. A. Radermacher[a], J. Magat[a], C. Bouzin[c], S. Laurent[b], T. Dresselaers[d], U. Himmelreich[d], S. Boutry[b], I. Mahieu[b], L. Vander Elst[b], O. Feron[c], R. N Muller[b], B. F. Jordan[a] and B. Gallez[a]*

The aim of this study was to determine the value of different magnetic resonance (MR) protocols to assess early tumor response to chemotherapy. We used a murine tumor model (TLT) presenting different degrees of response to three different cytotoxic agents. As shown in survival curves, cyclophosphamide (CP) was the most efficient drug followed by 5-fluorouracil (5-FU), whereas the etoposide treatment had little impact on TLT tumors. Three different MR protocols were used at 9.4 Tesla 24 h post-treatment: diffusion-weighted (DW)-MRI, choline measurement by ^{1}H MRS, and contrast-enhanced MRI using ultrasmall iron oxide nanoparticles (USPIO) targeted at phosphatidylserine. Accumulation of contrast agent in apoptotic tumors was monitored by T_2-weighted images and quantified by EPR spectroscopy. Necrosis and apoptosis were assessed by histology. Large variations were observed in the measurement of choline peak areas and could not be directly correlated to tumor response. Although the targeted USPIO particles were able to significantly differentiate between the efficiency of each cytotoxic agent and best correlated with survival endpoint, they present the main disadvantage of non-specific tumor accumulation, which could be problematic when transferring the method to the clinic. DW-MRI presents a better compromise by combining longitudinal studies with a high dynamic range; however, DW-MRI was unable to show any significant effect for 5-FU. This study illustrates the need for multimodal imaging in assessing tumor response to treatment to compensate for individual limitations. Copyright © 2011 John Wiley & Sons, Ltd.

Keywords: Tumor response; EPR; MRI; diffusion-weighted imaging; choline; MR spectroscopy; targeted contrast agent

INTRODUCTION

Strategies for anticancer treatment are based on type of cancer, location and grade of the tumor, stage of disease and general condition of the patient (1). For this reason, the best treatment for each individual patient needs to be determined. The prediction of tumor response to therapy is usually determined from measurements of tumor size based on morphological imaging results (2). However, tumor shrinkage can take several weeks to manifest. Therefore, early indication of tumor treatment response has become a major area of research. One method widely used in clinics relies on the decrease in [^{18}F]fluorodeoxyglucose uptake in treatment-sensitive tumors by positron emission tomography (3,4).

Imaging of apoptosis also allows early evaluation of treatment response in cancer patients. During early apoptosis, phosphatidylserine (PS) exposure on the outer leaflet of the cell membrane serves as a recognition signal for phagocytes (5). Radiolabeled annexin A5 has been most used in assessing apoptosis *in vivo*. Clinical trials using radiolabeled annexin A5 have been con-

* *Correspondence to: Prof. Bernard Gallez. Biomedical Magnetic Resonance Unit. Avenue Mounier, 73.40, B-1200 Brussels, Belgium. E-mail: bernard.gallez@uclouvain.be*

a *K. A. Radermacher, J. Magat, B. F. Jordan, B. Gallez Biomedical Magnetic Resonance Group, Louvain Drug Research Institute, Université Catholique de Louvain, Brussels, Belgium*

b *S. Laurent, S. Boutry, I. Mahieu, L. Vander Elst, R. N. Muller NMR and Molecular Imaging Laboratory, University of Mons, Mons, Belgium*

c *C. Bouzin, O. Feron Pole of Pharmacology and Therapeutics, Institute of Experimental and Clinical Research, Université Catholique de Louvain, Brussels, Belgium*

d *T. Dresselaers, U. Himmelreich Biomedical NMR Unit/MoSAIC, K.U . Leuven, Leuven, Belgium*

Abbreviations used: *5-FU, 5-fluorouracil; ADCw, apparent diffusion coefficient of water; CP, cyclophosphamide; CTL, control; DW, diffusion-weighted; EPR, electron paramagnetic resonance; ET, etoposide; FLASH, fast low angle shot; H&E, hematoxylin and eosin; PEG, polyethylene glycol; PRESS, point-resolved spectroscopy; PS, phosphatidylserine; RARE, rapid acquisition with relaxation enhancement; ROI, region of interest; SI, signal intensity; TLT, transplantable liver tumor; TUNEL, terminal deoxyribosyl transferase dUDP nick end labeling; USPIO, ultrasmall particles of iron oxide.*

ducted in cancer patients (6–10). Other compounds targeting early loss of cell membrane asymmetry and exposure of phosphatidylserine on the cell surface are peptides isolated by phage display (11–13) and the C2A domain of synaptotagmin 1 (14). The anionic nature of the PS molecules can be targeted by cationic liposomes (15) or by cationic coordination complexes (16,17). Other potential tracers are caspase-3 specific binding molecules (18,19) or small amphiphatic molecules of the aposense group that accumulate inside the cell from where they emit a fluorescent signal (20,21). The PS-targeting hexapeptide (E3) has been isolated by phage display on apoptotic murine livers and tested for its selectivity and binding capacity to PS (11). This peptide has been coupled to pegylated ultrasmall particles of iron oxides (USPIO), since it was previously demonstrated that USPIO pegylation was able to prolong blood circulation time and as a result, increase the possibility of achieving its target by decreased hepatic capture (22). This new MR contrast agent (USPIO-E3) has been tested *in vitro, ex vivo and in vivo* on irradiated transplantable liver tumors (23). Results from that study showed that, due to the targeted superparamagnetic particles, distinction between irradiated and control (CTL) tumors could be observed using magnetic resonance imaging (MRI) and electron paramagnetic resonance (EPR).

Other MR methods such as diffusion-weighted MRI (DW-MRI) and ^{1}H-MRS spectroscopy have been proposed to assess tumor response to treatments (24). Biophysical phenomena such as molecular diffusion can be useful in assessing cell viability and integrity (25). Physical boundaries such as cell membranes and subcellular structures restrict diffusion. DW-MRI can evaluate tumor response to radiation and chemotherapy (26–29). Biochemical processes such as metabolism of membrane choline can be monitored by MR spectroscopy in tumors *in vivo* to provide metabolic information on tumor cell proliferation and membrane degeneration (30–32). High levels of choline containing compounds have been observed in tumors by *in vivo* ^{31}P- and ^{1}H-MRS (33–35) that can be reversed after successful treatment. Choline is being explored as a biomarker for tumor diagnosis, staging and clinical response monitoring (36,37).

Because there is a critical need for comparing the respective values of imaging biomarkers that may early assess the response of tumors to cytotoxic treatments, this study was designed to compare various MR methods applied to a one-tumor model that presents various degrees of response to different chemotherapeutic agents (cyclophosphamide, 5-fluorouracil and etoposide). We compared DW-MRI, ^{1}H-MRS and the recently developed contrast agent USPIO-E3 targeted at phosphatidylserine.

METHODS AND MATERIALS

Animals

Syngeneic transplantable liver tumors (TLT) were induced in the gastrocnemius muscle of 5-week-old male NMRI mice (Elevage Janvier, France) (38). For inoculation, approximately 10^6 cells in 0.1 ml of media were injected intramuscularly into the right leg of the mice. Mice developed palpable tumors within one week of inoculation. Mice were divided into four groups: one untreated control (CTL) group and three treatment groups. When the hind leg diameter reached 8 ± 0.5 mm, mice were either treated with cyclophosphamide (CP: 160 mg/kg IP with 5-fluorouracil (5-FU: 100 mg/kg IP) or with etoposide (ET: 20 mg/kg IP).

Cytotoxic agents used in this study were obtained from St. Luc Hospital (Brussels, Belgium). USPIO-E3 particles were prepared from nanoparticles with carboxylated groups on the surface as previously described (39). USPIO particles were functionalized in two successive steps with the E3 peptide (TLVSSL, Neomps, Strasbourg, France) and then with an amino-PEG 750 (Fluka, Bornem, Belgium). Characterization of the contrast probe has previously been described (23). For EPR and T_2-weighted MRI experiments, the contrast agent was intravenously injected (7.7 mg Fe/kg) 21 h after injection of the respective treatment. The procedure was approved by a local ethics review committee according to national animal care regulations.

Tumor growth delay and survival curve

At day 0, tumor-bearing mice (n=8-9/group) were intraperitonealy injected with one of the chemotherapeutic drugs or remained untreated. The diameter of the hind leg was measured daily to visualize a potential tumor growth delay occurring after treatment. When the rear leg diameter reached 15 mm, the mice were sacrificed and that particular day was considered as the endpoint of the survival curve.

USPIO-E3 quantification by EPR

Iron oxide particles were injected into the tail vein of mice 21 h after injection of the chemotherapeutic agent. The animals (n=10-11/group) were sacrificed three hours after contrast agent injection and tumors were excised and weighted. The tumors were freeze-dried and crushed into a fine powder, which was then weighted and placed into the X-band EPR cavity. We calculated the iron oxide content of each tumor by comparison with a calibration curve. The instrument settings were: frequency, 9.4 GHz; microwave power, 5.05 mW; center field, 3150 G; field width, 5000 G; modulation amplitude, 30.81 G; time constant, 20.48 ms; conversion time, 20.48 ms; modulation field, 100 kHz; total acquisition time, 83 s. Measurements were performed at room temperature.

MR

MR experiments were performed using the same 9.4 T small animal Biospec MR system (Bruker, Ettlingen, Germany) equipped with a 20 cm horizontal bore, a whole body transmitter and a surface coil receiver for signal reception. The animals (n=4-5/group) were anesthetized by isoflurane inhalation 4% in O_2 for initiation and 1-2% in O_2 for maintenance (isoflurane was provided by St. Luc Hospital, Brussels, Belgium) and their hind legs were fixed by clay. Animals were laid on a warm waterbed to maintain body temperature at 37 °C. A temperature probe was inserted into the rectum and a pressure cushion was placed near the chest to monitor respiration. Positioning of the mice was verified using a FLASH MRI sequence in three directions of the space (TR/TE: 3000/200 ms). A T_2-weighted axial turbo spin-echo RARE sequence (TR/TE, 3500/9.065 ms; effective TE, 27.20 ms; RARE factor, 7) was used to provide anatomical images of the mice.

T_2-weighted MRI and T_2 measurements

A multi spin-echo sequence was applied for accurate assessment of signal intensities (SI) and T_2 relaxation times before and three hours after contrast agent injection as follows: TR/TE, 2500/10 ms; number of echoes, 16; echo spacing, 10 ms; slices, 7; slice thickness, 1 mm; interslice distance, 1.5 mm; in-plane resolution,

0.117 mm^2/pixel; acquisition time, 8 min. Mean SI of the tumors was measured within manually drawn regions of interest (ROI) on images from the seventh echo (TE, 70 ms) of the multi-echo sequence and normalized to the noise using a MATLAB® program (version 7.9). Mean T_2 relaxation times for tumors were also calculated from the multi spin-echo datasets using MATLAB. T_2 values were obtained by an exponential fit of the signal amplitudes *versus* echo time. T_2 maps were established on a pixel-by-pixel basis in the ROI.

Diffusion-weighted imaging

For DW-MRI, a transverse echo planar imaging sequence was used with the following acquisition parameters: TR/TE, 3000/27.96 ms; duration of diffusion gradients (δ), 7 ms; separation of diffusion gradients (Δ), 14 ms; slice number, 7; slice thickness, 1 mm; interslice distance, 1.5 mm; in-plane resolution, 0.234 mm^2/pixel; acquisition time, 4 min 12 s. DW images were acquired using b values of 0, 200, 400, 600, 800 and 1000 s/mm^2. The b value is equal to $\gamma^2 G_d{}^2 \delta^2 (\Delta - (\delta/3))$, where G_d is the strength of the diffusion weighting gradient and γ is the gyromagnetic ratio for protons. Mean apparent diffusion coefficient (ADCw) and ADCw maps were calculated from the DW images. Using MATLAB, the exponential decay of signal as a function of the b-value was measured according to the Stejskal-Tanner equation $S = S_0 e^{-bADCw}$, where S_0 is the signal intensity achieved without gradient and S is the signal intensity with diffusion weighting.

Single voxel ^{1}H MRS

For single voxel spectroscopic data acquisition, voxel localization was performed on the corresponding anatomical images obtained by the FLASH and turbo RARE sequences. Proton MR spectra were acquired using a PRESS sequence (TR/TE; 2500/15 ms). Voxel size of $2 \times 2 \times 2$ mm^3 and 256 averages were used for MRS studies in all cases. The water-fat shift was 0.52 mm and a spectral resolution of 0.98 Hz/point was achieved. Spatially localized saturation bands were used to suppress signals from surrounding areas (gap to voxel: 0.5 mm). Field homogeneity was optimized over the selected volume of interest by shimming on the water signal for each tumor to a line width of < 20 Hz. Automatic shimming and water suppression (VAPOR) were used. Acquisition time for spectroscopic studies was about 11 min.

MR data analysis

Review of T_2-weighted and DW images was performed on an independent workstation using MATLAB software to define ROIs. The same program was used to establish signal intensity, T_2 and ADCw maps, and to calculate signal loss, transversal relaxation time T_2 and mean ADCw values. Signal intensities, T_2 and ADCw values were determined and averaged for every slice where the tumor was found. MR spectra were also analyzed on an independent workstation using Topspin software (version 2.0, Bruker Biospin, Rheinstetten, Germany). For data processing, Fourier transformation, 5 Hz linebroadening and phase and baseline corrections were applied. Peak areas were measured for choline peak (at 3.21 ppm). Metabolic ratios were calculated based on measurements of the unsuppressed water peak area. Results were finally expressed as percentage compared to the values obtained for the untreated CTL mice to allow easier comparison between the MR methods used.

Histology

Tumor bearing animals were treated with CP, 5-FU, ET or remained untreated, and tumors were excised 24 h post-treatment. Tumors (n = 3/group) were either fixed in 4% paraformaldehyde for standard paraffin sections or embedded in O.C.T.® compound for cryosectioning. In both cases, samples were cut into 5 μm sections. The paraffin sections were stained with H&E and photographed on a Zeiss MIRAX microscope for a global overview of the necrotic regions in the tumors. The frozen slices were probed for apoptosis by TUNEL assay using a commercially available *in situ* cell death detection kit (Roche Diagnostics, Vilvoorde, Belgium). Nuclei were also counterstained with 4,6-diamidino-2-phenylindole (DAPI). Slides were photographed using a Zeiss Axioskop (Vertrieb, Germany) microscope equipped for fluorescence. Quantification of necrotic and apoptotic regions expressed as percentage of the whole tumor area was obtained using Image J.

Statistical analysis

All values were expressed as mean ± standard error. A logrank test was used to compare the survival curves. For T_2–weighted and diffusion-weighted acquisitions, six slices per tumor were acquired. The six mean signal intensities, T_2 and ADCw values that were then generated were averaged for each mouse, and statistical differences between the groups, were further compared with two-way ANOVA. A p-value > 0.05 was considered significant. The following symbols are used in the figures: $\star P \leq 0.05$, $\star\star P \leq 0.01$, $\star\star\star P \leq 0.001$.

RESULTS

Tumor growth delay and survival curve

The chemosensitivity of TLT tumors to the different cytotoxic drugs (cyclophosphamide CP, 5-fluorouracil 5-FU, etoposide ET) was compared by tumor growth delay and by evaluating survival after treatment (Figs. 1A and B). As shown in Figures 1A and B, the response was higher when using CP compared to 5-FU; the response to 5-FU being higher than for ET. The ET curve was almost superimposed to the one obtained for the CTL tumors. As a result, the impact of ET treatment on these tumors at the dose of 20 mg/kg was minimal. Compared to the CTL group, survival was significantly higher for the CP-treated group ($p \leq 0.001$), significant for the 5-FU-treated group ($p \leq 0.05$) and non-significant for the ET-treated group (Fig. 1B).

USPIO-E3 quantification by EPR

X-band EPR was used to quantify the accumulation of the targeted iron oxide particles. The amount of USPIO-E3 particles in excised TLT tumors was measured 3 h after injection of the contrast agent and 24 h after treatment administration (Fig. 2). The signal intensity of the iron oxide spectrum acquired in excised tumors was correlated to a previously established calibration curve (data not shown). The accumulation of the cell death-targeted USPIOs was significantly higher in CP- and 5-FU-treated tumors (74 ± 7 ng/mg and 64 ± 9 ng/mg, respectively) than in ET-treated and CTL tumors (40 ± 5 ng/mg and 33 ± 6 ng/mg, respectively).

T_2-weighted MRI and T_2 measurements

To examine whether USPIO-E3 might serve as a selective MR contrast agent for cell death, mice were imaged 24 h after

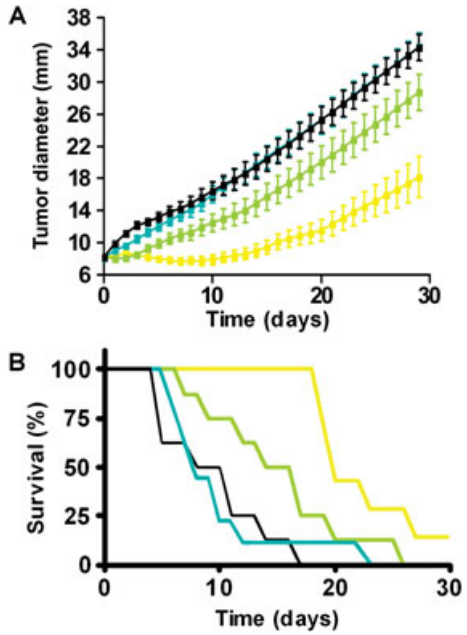

Figure 1. (A) Tumor growth curves of mice with TLT tumors treated with cyclophosphamide (yellow), 5-fluorouracil (green), etoposide (blue) or untreated (black). The treatment was injected at a tumor size of 8±0.5 mm (n=8-9/group). Data are presented as the average tumor diameter for each group *versus* time from start of treatment. (B) Survival curves of mice with untreated TLT tumors (black line) or mice with tumors either treated with CP (yellow line), 5-FU (green line) or ET (blue line). When tumor diameters reached 15 mm, mice were sacrificed, which was considered as the endpoint of the survival study.

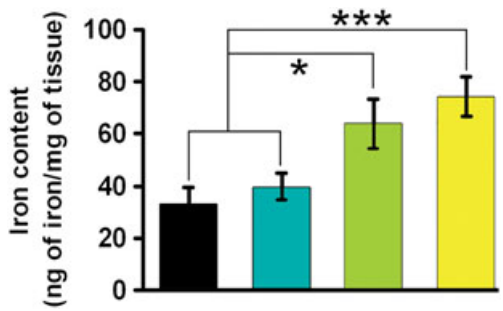

Figure 2. Accumulation of iron oxide particles (expressed in ng of iron per mg of tumor tissue) in TLT hepatocarcinomas as measured *ex vivo* by X-band EPR (n=10-11/group). EPR spectra of the different tumors were recorded 24 h after IP injection of chemotherapeutic treatment and 3 h after IV injection of the contrast agent USPIO-E3. Yellow bars represent animals injected with CP, green bars represent tumors treated with 5-FU and blue bars represent ET treatment. Untreated tumors served as control (black bars).

injection of the chemotherapeutic drugs. MR images were obtained before and 3 h after IV injection of USPIO-E3 particles. On all post contrast images, a signal decrease was observed in treated and CTL tumors (Figs. 3A and B). However, signal loss was more pronounced after CP- and 5-FU treatment than after ET treatment or in CTL tumors. The signal loss normalized to the noise and expressed as a percentage compared to the signal loss of untreated CTL tumors is shown in Figure 3C. Three hours after administration of the PS-targeted contrast probe, signal loss was −11±1% for CP-treated animals, -3±2% for 5-FU-treated mice and −1±2% for the ET-treated mice when compared to the untreated tumors. To confirm these results, T_2 maps were established for each tumor slice (Fig. 4A) and mean T_2 values were obtained from tumors before and 3 h after administration of USPIO-E3 (Figs. 4A and B). When compared to the T_2 shortening of CTL tumors, T_2 shortening in CP-treated tumors was approximately −11±1%, -5±2% in 5-FU-treated mice and 1±2% in ET-treated mice compared to CTL tumors (Fig. 4C). The results are consistent with those obtained for tumor signal loss.

Diffusion-weighted imaging

After the use of an efficient anticancer treatment, tumor cellularity should be reduced and should result in an increase in the apparent diffusion coefficient of water (ADCw). In fact, ADCw maps showed a higher intensity 24 h after CP- and 5-FU treatment when compared to the inefficient ET treatment or to CTL tumors (Fig. 5A). When average ADCw values of tumors were compared pre- and 24-h post-treatment (Fig. 5B), a reduction in ADCw was observed for inefficient etoposide treatment and for untreated CTL tumors; whereas, the ADCw value remained the same after 5-FU-treatment and even increased after CP treatment, representing a loss in tumor cellularity. ADCw values were also compared to the ADC of CTL tumors. As shown in Figure 5c, mean ADCw values were the highest in CP-treated tumors (37±4%) followed by the 5-FU-treated mice (18±8%); the lowest value was obtained for ET-treated mice (10±6%).

Single Voxel ^{1}H MRS

Figure 6A displays typical ^{1}H-MR spectra obtained from tumor bearing mice before and 24 h after CP treatment. It can be observed that the total choline peak is slightly decreased for the post-treatment compared to the pre-treatment spectrum. The choline peak areas were normalized to the corresponding unsuppressed water signal and then again compared to the CTL group (Fig. 6B). CP- and 5-FU-treated animals showed a higher decrease in choline peak area after treatment (−19±22% and −18±5%, respectively) than ET-treated and CTL mice (−10±14% and 0±4%, respectively). However, because of the high standard error of the data obtained from the CP group, only the 5-FU-treated group was significantly different compared to the CTL group.

Histology

Figure 7 displays representative tumor slices after TUNEL (left column) and H&E (right column) staining for quantification of apoptosis and necrosis, respectively. TUNEL staining of untreated and treated tumors clearly shows an increase in positively stained cells after CP- and 5-FU treatment (26±8% and 21±4%, respectively) than after ET treatment (10±5%) or of that in CTL tumors (0.5±0.4%). For quantification of necrosis, areas occupied by necrotic regions were measured on H&E stained slices. None of the three chemotherapeutic drugs was able to increase the initial level of necrosis compared to the CTL tumor, where 20±4% of the tumor area displayed necrotic features (CP, 20±4%; 5-FU, 21±1%; and ET, 23±3%).

DISCUSSION

The activity of different clinically relevant chemotherapeutic drugs (cyclophosphamide, 5-fluorouracil and etoposide) was evaluated

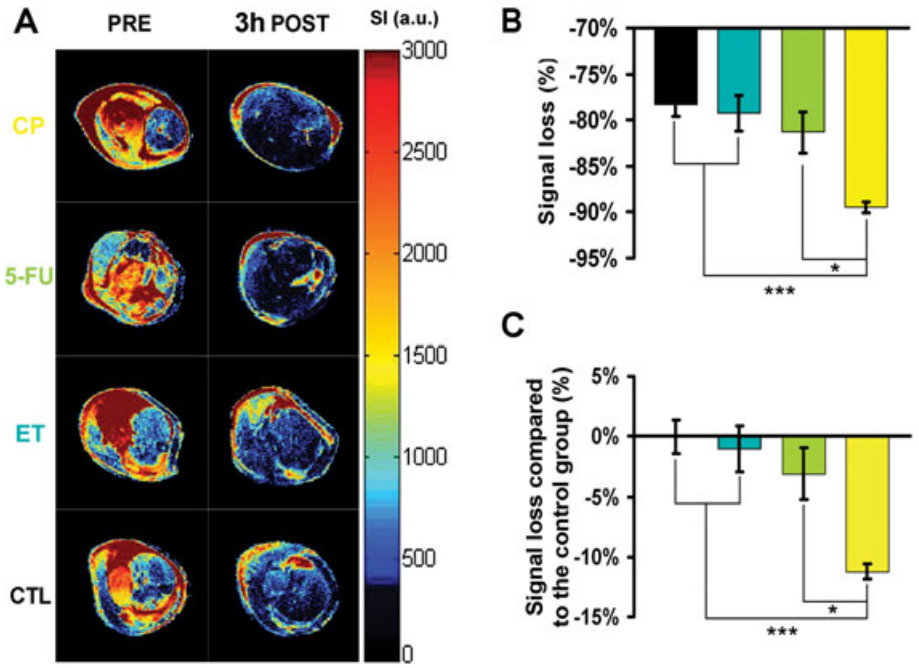

Figure 3. (A) Twenty-four h after injection of the cytotoxic drug, axial T_2-weighted MR images of murine tumors obtained before and 3 h after USPIO-E3 administration (n=4.5/group). (B) Three hours after USPIO-E3 injection, mean negative contrast enhancement values were obtained from regions of interest that encompassed the entire tumor region on T_2-weighted MR images. Signal loss of the CP (yellow bars), 5-FU (green bars), ET (blue bars) and untreated (black bars) groups was expressed as percentage of the pre-contrast signal. C) Signal loss expressed as percentage compared to untreated CTL tumors.

on TLT tumor models using a cell-death targeted MR contrast agent DW-MRI and single voxel ^{1}H MR spectroscopy of choline. Tumor growth delay and survival curves were established first to evaluate the impact of the treatment. Etoposide treatment had almost no effect on these tumors and mice died at the same rate than untreated tumor bearing mice. 5-fluorouracil treatment induced a short delay in tumor growth and cyclophosphamide was the most efficient treatment (two of nine were cured). Overall, this offered a panel of tumor responses to evaluate the efficacy of MR methods to early assess response to a treatment.

USPIO-E3 particles induced considerable signal loss on T_2-weighted MR images due to strong magnetic susceptibility

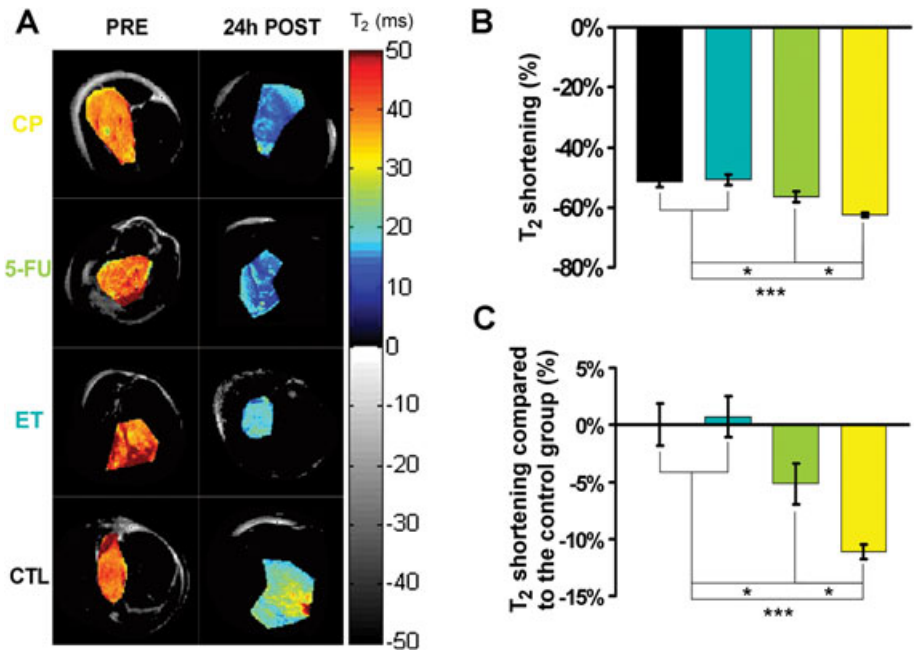

Figure 4. (A) T_2-weighted multi-echo acquisitions allowed generation of T_2 maps in which each pixel represents the spatially localized T_2 value of the tumor. (B) Shortening of T_2 relaxation times in treated and CTL tumors 3 h after injection of the contrast material (CP, yellow bars; 5-FU, green bars; ET, blue bars and CTL, black bars). (C) The graph shows mean T_2 shortening expressed as percentage of the T_2 reduction obtained in CTL mice.

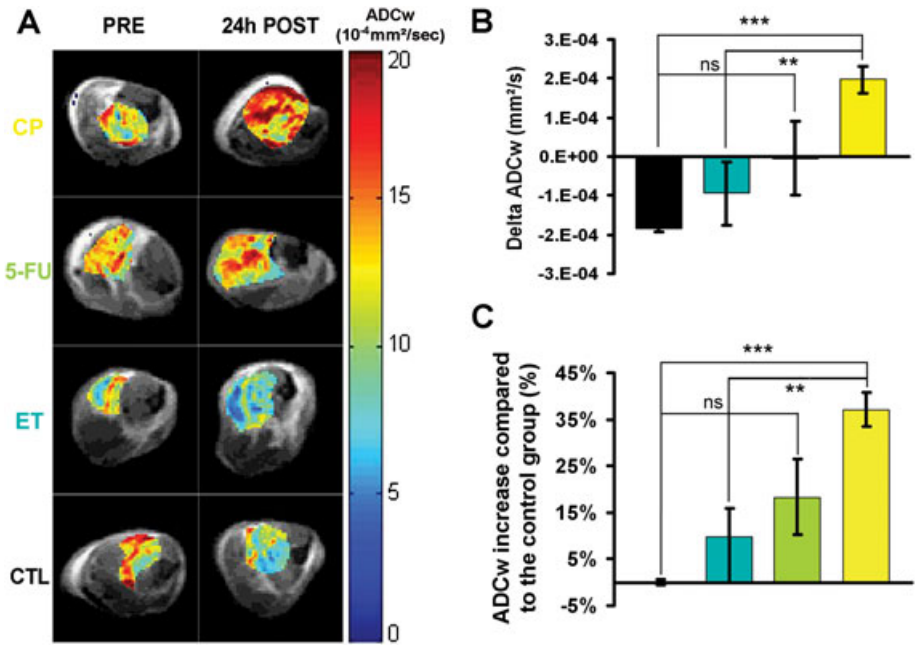

Figure 5. (A) ADCw maps of tumor bearing mice before and 24 h after injection of the treatment. Each image represents an axial DW image (b-value = 0) of the mouse leg with the tumor area transformed as an ADCw map. (B) Delta of the average tumor ADCw observed pre- and 24-h post-treatment (CP, yellow bars; 5-FU, green bars; ET, blue bars and CTL, black bars). (C) Tumor ADCw value expressed as percentage of the ADCw obtained for of untreated CTL tumors.

effects. We also used EPR spectrometry as a highly sensitive method to quantify the iron oxide content in the tumor without any interference from background (22,40,41). The iron oxide content in tumors was correlated with signal loss and T_2 shortening measured on T_2-weighted MR images pre- and post-contrast. For both techniques, we observed statistically significant differences between the most successfully treated groups (CP and 5-FU) and the CTL group or the group treated inefficiently by etoposide. However, there was a large iron oxide accumulation in untreated CTL tumors, resulting in an important decrease in signal intensity. Overall, although significant, the difference in loss of signal intensity between responsive and unresponsive tumors was relatively small. It is important to note that images were acquired three hours after injection of the contrast agent. This time point was chosen based on our previous study that showed sufficient clearance form the blood and enough sensitivity to discriminate between irradiated and untreated tumors (23). However, this time point remains arbitrary. It would be interesting to generate data at longer time points after injection of the contrast agent to determine whether or not more significant differences between treatments can be obtained.

Although the data do not match perfectly between EPR and TUNEL assays, both techniques show similar trends of response between treatments. The main difference between the two techniques is in the difference between CTL and treated tumors where it is more pronounced using TUNEL assay instead of EPR because of the non specific accumulation of USPIO particles in non treated tumors (see below).

In our previous study, we found that USPIO-E3 particles presented a much higher affinity for dying cells treated *in vitro* by staurosporine or *in vivo* by irradiation than USPIOs grafted with a scrambled peptide or ungrafted USPIOs (23). However, the accumulation of USPIO-E3 in untreated or in unresponsive tumors is likely due to a non-selective uptake by macrophages involved in tumor related inflammation and to a large basal necrosis present in tumors before treatment. The level of necrosis was about 20% in untreated TLT tumors, as shown by H&E histological staining. Since cell membrane integrity is lost during necrosis; the PS molecule becomes accessible and USPIO-E3 potentially targets necrotic cells. In practice, the basal uptake by untreated tumors could lead to uncertainty in determining areas with poor local response in tumors. Another possible explanation for non-specific USPIO accumulation in tumors is the enhanced permeation and retention (EPR effect). Nanoparticles are known to passively diffuse and accumulate at sites with excessively leaky vasculature such as in tumors, regardless of whether the tumors are undergoing apoptosis or not. A parameter that requires further investigation in future studies is the time needed to observe the washout of the USIO-E3 from the tumor to determine the frequency of injection of the contrast agent for chronic monitoring of cell death.

DW-MRI is completely non-invasive and relies on intrinsic contrast mechanisms rather than injection of a contrast agent. This characteristic allows early monitoring of tumor response to treatment (42,43). In our tumor model, CP induced a substantial increase in ADCw 24 h after treatment, reflecting an increase in extracellular water fraction; while changes in ADCw were not significantly different after 5-FU treatment and ADCw even decreased in ET- and untreated tumors. The increase in ADCw was correlated to the induction of apoptosis while the level of necrosis remained unchanged after treatment. Still, this is likely a particular case, since ADCw is unlikely to differentiate between necrosis and apoptosis. Increases in ADCw reflect an increase in the mobility of water, either through loss of membrane integrity or by an increase in the proportion of total extracellular fluid with a corresponding decrease in cellular size or number as observed in necrosis or apoptosis (42).

NMR IN BIOMEDICINE

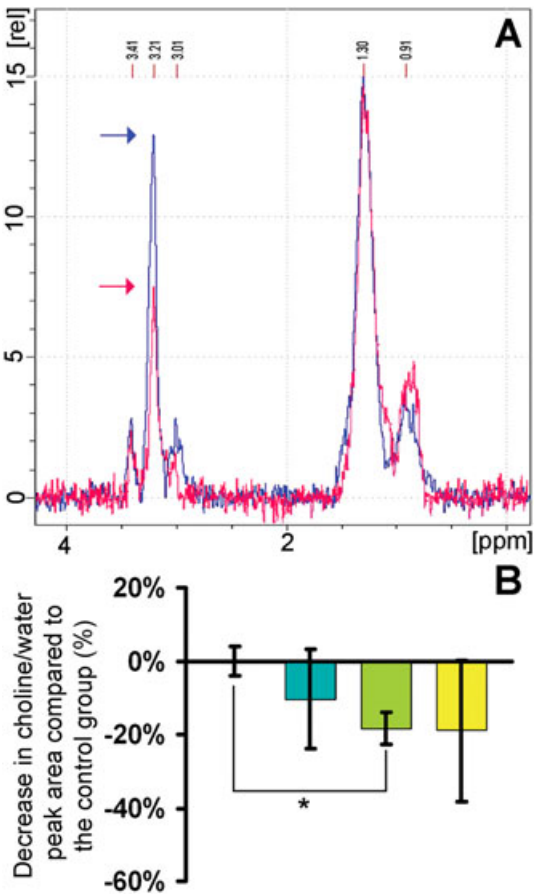

Figure 6. (A): *In vivo* ^{1}H-MR spectra obtained from murine TLT tumors before (blue spectrum) and 24 h after cyclophosphamide treatment (pink spectrum). In addition to the total choline peak situated at 3.21 ppm, other peaks displayed on the spectrum were the lipid peaks (0.91 and 1.30 ppm), the creatine peak (3.01 ppm) and the taurine peak (3.41 ppm). The presence of creatine and taurine suggests that at least in part, intact muscle tissue was also present in these spectra. (B) Evolution of the choline peak before and 24 h after tumor treatment. The choline peak area is expressed as a choline to water ratio and as percentage of the ratio obtained for CTL mice. (CP, yellow bars; 5-FU, green bars and ET, blue bars).

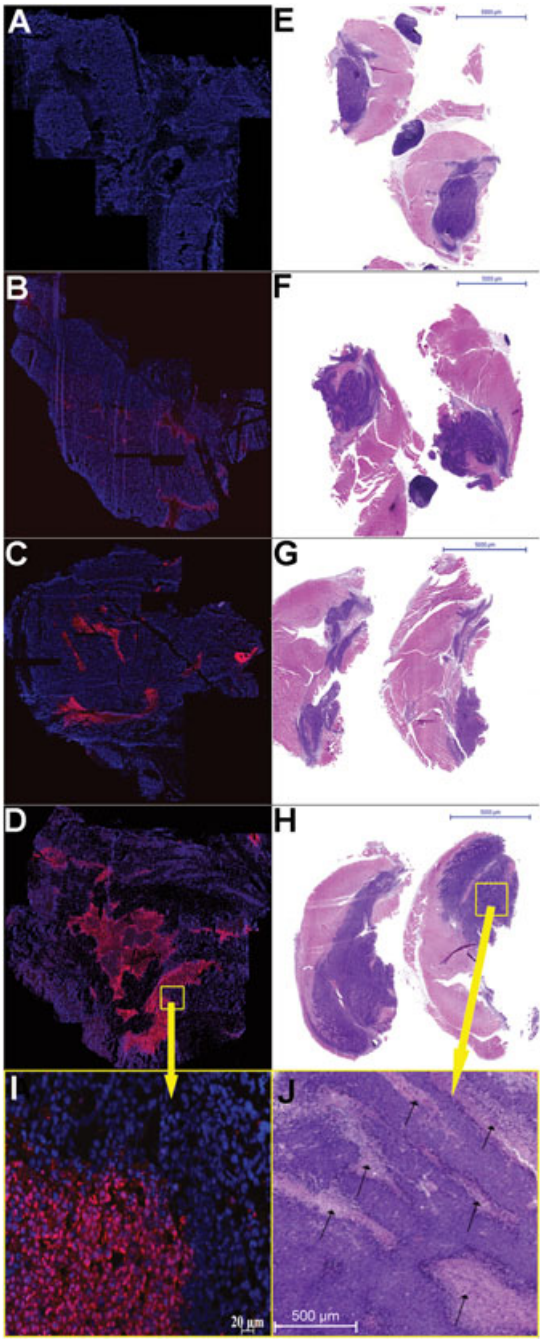

Figure 7. Representative histological stainings performed on tumor slices. Fluorescent TUNEL stained section from untreated mice (A) and from tumors 24 h after etoposide (B), 5-fluorouracil (C) and cyclophosphamide (D) treatment. TUNEL-positive nuclei are stained in red and the nuclear counterstain DAPI in blue (magnification, 50 x). H&E stained section from untreated mice (E) and from mice 24 h after etoposide (F), 5-fluorouracil (G), and cyclophosphamide (H) treatment. Only tumor regions were used for quantification of necrosis; the surrounding muscle tissue was not taken into account. Figures (I) and (J) represent magnificated areas (yellow squares) from CP-treated tumors after TUNEL and H&E staining, respectively. Black arrows on Figure J indicate necrotic regions of the tumor.

In vivo MRS can be used repeatedly and non-invasively to measure the metabolite content of tumors in living animals or patients. Elevation of the choline peak is thought to represent membrane phospholipid synthesis and therefore reflects cellular proliferation and cell density occurring during progression of cancer. In necrotic tumors, release of glycerophosphocholine due to cell membrane degradation contributes to increased tCho concentrations. The usefulness of choline ^{1}H-MRS in evaluating response to treatment has been reported in different tumor types in patients (44,45). In the present investigation, mean choline to water ratios were higher for CTL tumors than for treated tumors, although this difference was not significant. When analyzing each mouse individually, we did not find a systematic decrease in the choline peak after efficient treatment. The SD for choline levels was quite large, especially in treated tumors.

In this study, the amount of choline related compounds was assessed with the ratio method by using the unsuppressed water peak as an internal standard. However, this method has its limitations because tumor water content is highly variable. An additional critical factor is the timing used. We cannot exclude that a longer follow-up after treatment could possibly show a more distinct decrease in choline peak areas after therapy. Seierstad *et a*. (46)

reported similar results 24 h after irradiation of HT29 xenografts and explained the increase of choline metabolites by a breakdown of cell membrane constituting lipids. Another explanation is that during necrosis, almost all metabolites, including choline, increase (47). Another limitation of ^{1}H single voxel MRS is the lack of spatial resolution of this method applied over a heterogeneous tissue. Multi voxel imaging could be a better method for future evaluation to account for heterogeneity of the tumor. Finally, even though choline has been identified as a surrogate marker for some classic cytotoxic therapies and for drugs with specific molecular targets such as HIF-1alpha, choline kinase or PI3K (48) unexpected opposite effects on tCho were observed following inhibition of HSP90 or HDAC, two broad spectrum inhibitors. tCho changes could, therefore, not necessarily mirror the changes associated with the downstream signaling pathways of specific inhibitors (48). This illustrates the complexity of interpretation of the choline peak as a marker of response to treatment that is not likely to be universal for all therapies.

When comparing the change in parameters of CP-treated mice relative to controls (the dynamic range), there was a difference of 37% for DW-MRI of 19% for choline spectroscopy and 11% for T_2-weighted MRI. Even though the dynamic range was the lowest for cell death detection by USPIO-E3 particles, this technique was more reliable than choline spectroscopy because differences were significant. Our MRS results showed significant variations, which makes it impossible to be conclusive. ADCw was found to be the most sensitive and reliable early marker of tumor response after chemotherapy treatment. It would be interesting to combine two or three protocols into one MR session to gain insights into the complex tumor response. However, no single technique is completely reliable and each of these techniques has its limitations. An interesting perspective could be to determine the value of each marker of response at different time points since the dynamic range could vary over time after starting cytotoxic treatment. Finally, additional tumor models should be considered to draw a robust conclusion in terms of comparison of techniques since response to chemotherapeutic agents can vary from one tumor model to another and cell death markers do not always show the same relevance on various tumor types (i.e. especially for choline).

Acknowledgements

This study was supported by grants from the Belgian National Fund for Scientific Research (FNRS); Televie grants (7.4547.08); the Fonds Joseph Maisin; the Saint-Luc Foundation; the Fondation contre le Cancer; the Actions de Recherches Concertées-Communauté Française de Belgique-ARC 09/14-020 and 05/10-335; and the Pôle d'attraction Interuniversitaire PAI VI (P6/38 and P6/29).

REFERENCES

1. De Saint-Hubert M, Prinsen K, Mortelmans L, Verbruggen A, and Mottaghy FM. Molecular imaging of cell death. Methods, 2009; 48: 178–187.
2. Therasse P, Arbuck SG, Eisenhauer EA, Wanders J, Kaplan RS, Rubinstein L, Verweij J, Van Glabbeke M, van Oosterom AT, Christian MC, and Gwyther SG. New guidelines to evaluate the response to treatment in solid tumors. European Organization for Research and Treatment of Cancer, National Cancer Institute of the United States, National Cancer Institute of Canada. J. Natl. Cancer Inst. 2000; 92: 205–216.
3. Chaiken L, Rege S, Hoh C, Choi Y, Jabour B, Juillard G, Hawkins R, and Parker R. Positron emission tomography with fluorodeoxyglucose to evaluate tumor response and control after radiation therapy. Int. J. Radiat. Oncol. Bio. Phys. 1993; 27: 455–464.
4. Berlangieri SU, Brizel DM, Scher RL, Schifter T, Hawk TC, Hamblen S, Coleman RE, and Hoffman JM. Pilot study of positron emission tomography in patients with advanced head and neck cancer receiving radiotherapy and chemotherapy. Head Neck, 1994; 16: 340–346.
5. Fadok VA, Voelker DR, Campbell PA, Cohen JJ, Bratton DL, and Henson PM. Exposure of phosphatidylserine on the surface of apoptotic lymphocytes triggers specific recognition and removal by macrophages. J. Immunol. 1992; 148: 2207–2216.
6. Blankenberg F, Mari C, and Strauss HW. Imaging cell death *in vivo*. Q. J. Nucl. Med. 2003; 47: 337–348.
7. Haas RL, de Jong D, Valdés Olmos RA, Hoefnagel CA, van den Heuvel I, Zerp SF, Bartelink H, and Verheij M. *In vivo* imaging of radiation-induced apoptosis in follicular lymphoma patients. Int. J. Radiat. Oncol. Biol. Phys. 2004; 59: 782–787.
8. Kartachova M, Haas RL, Olmos RA, Hoebers FJ, van Zandwijk N, and Verheij M. *In vivo* imaging of apoptosis by 99mTc-Annexin V scintigraphy: visual analysis in relation to treatment response. Radiother. Oncol. 2004; 72: 333–339.
9. Vermeersch H, Loose D, Lahorte C, Mervillie K, Dierckx R, Steinmetz N, Vanderheyden JL, Cuvelier C, Slegers G, and Van de Wiele C. 99mTc-HYNIC Annexin-V imaging of primary head and neck carcinoma. Nucl. Med. Commun. 2004; 25: 259–263.
10. Belhocine T, Steinmetz N, Green A, and Rigo P. *In vivo* imaging of chemotherapy-induced apoptosis in human cancers. Ann. N. Y. Acad. Sci. 2003; 1010: 525–529.
11. Laumonier C, Segers J, Laurent S, Michel A, Coppée F, Belayew A, Elst LV, and Muller RN. A new peptidic vector for molecular imaging of apoptosis, identified by phage display technology. J. Biomol. Screen. 2006; 11: 537–545.
12. Thapa N, Kim S, So IS, Lee BH, Kwon IC, Choi K, and Kim IS. Discovery of a phosphatidylserine-recognizing peptide and its utility in molecular imaging of tumour apoptosis. J. Cell. Mol. Med. 2007; 12: 1649–1660.
13. Hong HY, Choi JS, Kim YJ, Lee HY, Kwak W, Yoo J, Lee JT, Kwon TH, Kim IS, Han HS, and Lee BH. Detection of apoptosis in a rat model of focal cerebral ischemia using a homing peptide selected from *in vivo* phage display. J. Control Release, 2008; 131: 167–172.
14. Zhao M, Beauregard DA, Loizou L, Davletov B, and Brindle KM. Non-invasive detection of apoptosis using magnetic resonance imaging and a targeted contrast agent. Nat. Med. 2001; 7: 1241–1244.
15. Bose S, Tuunainen I, Parry M, Medina OP, Mancini G, and Kinnunen PK. Binding of cationic liposomes to apoptotic cells. Anal. Biochem. 2004; 331: 385–394.
16. Hanshaw RG, Lakshmi C, Lambert TN, Johnson JR, and Smith BD. Fluorescent detection of apoptotic cells by using zinc coordination complexes with a selective affinity for membrane surfaces enriched with phosphatidylserine. Chembiochem. 2005; 6: 2214–2220.
17. Quinti L, Weissleder R, and Tung CH. A fluorescent nanosensor for apoptotic cells. Nano. Lett. 2006; 6: 488–490.
18. Bullok KE, Gammon ST, Violini S, Prantner AM, Villalobos VM, Sharma V, and Piwnica-Worms D. Permeation peptide conjugates for *in vivo* molecular imaging applications. Mol. Imaging, 2006; 5: 1–15.
19. Zhou D, Chu W, Rothfuss J, Zeng C, Xu J, Jones L, Welch MJ, and Mach RH. Synthesis, radiolabeling, and *in vivo* evaluation of an 18F-labeled isatin analog for imaging caspase-3 activation in apoptosis. Bioorg. Med. Chem. Lett. 2006; 16: 5041–5046.
20. Cohen A, Ziv I, Aloya T, Levin G, Kidron D, Grimberg H, Reshef A, and Shirvan A. Monitoring of chemotherapy-induced cell death in melanoma tumors by N,N'-Didansyl-L-cystine. Technol. Cancer. Res. Treat. 2007; 6: 221–234.
21. Reshef A, Shirvan A, Waterhouse RN, Grimberg H, Levin G, Cohen A, Ulysse LG, Friedman G, Antoni G, and Ziv I. Molecular imaging of neurovascular cell death in experimental cerebral stroke by PET. J. Nucl. Med. 2008; 49: 1520–1528.
22. Radermacher KA, Beghein N, Boutry S, Laurent S, Vander Elst L, Muller RN, Jordan BF, and Gallez B. *In vivo* detection of inflammation using pegylated iron oxide particles targeted at E-selectin: a multimodal approach using MR imaging and EPR spectroscopy. Invest. Radiol. 2009; 44: 398–404.
23. Radermacher KA, Boutry S, Laurent S, Vander Elst L, Mahieu I, Bouzin C, Magat J, Gregoire V, Feron O, Muller RN, Jordan BF, and Gallez B. Iron Oxide Particles Covered with Hexapeptides Targeted at Phosphatidylserine as MR Biomarkers of Tumor Cell Death. Contrast Media Mol. Imaging, 2010; 5: 258–267.

24. Brindle KM. Detection of apoptosis in tumors using magnetic resonance imaging and spectroscopy. Adv. Enzyme Regul. 2002; 42: 101–112.
25. Moseley ME, Cohen Y, Mintorovitch J, Chileuitt L, Shimizu H, Kucharczyk J, Wendland MF, and Weinstein PR. Early detection of regional cerebral ischemia in cats: comparison of diffusion- and T2-weighted MRI and spectroscopy. Magn. Reson. Med. 1990; 14: 330–346.
26. Lidar Z, Mardor Y, Jonas T, Pfeffer R, Faibel M, Nass D, Hadani M, and Ram Z. Convection-enhanced delivery of paclitaxel for the treatment of recurrent malignant glioma: a phase I/II clinical study. J. Neurosurg. 2004; 100: 472–479.
27. Charles-Edwards EM and de Souza NM. Diffusion-weighted magnetic resonance imaging and its application to cancer. Cancer Imaging, 2006; 13: 135–143.
28. Deng J, Miller FH, Rhee TK, Sato KT, Mulcahy MF, Kulik LM, Salem R, Omary RA, and Larson AC. Diffusion-weighted MR imaging for determination of hepatocellular carcinoma response to yttrium-90 radioembolization. J. Vasc. Interv. Radiol. 2006; 17: 1195–1200.
29. Jordan BF, Runquist M, Raghunand N, Baker A, Williams R, Kirkpatrick L, Powis G, and Gillies RJ. Dynamic contrast-enhanced and diffusion MRI show rapid and dramatic changes in tumor microenvironment in response to inhibition of HIF-1alpha using PX-478. Neoplasia, 2005; 7: 475–485.
30. Szwergold BS. NMR spectroscopy of cells. Annu. Rev. Physiol. 1992; 54: 775–798.
31. Fulham MJ, Bizzi A, Dietz MJ, Shih HH, Raman R, Sobering GS, Frank JA, Dwyer AJ, Alger JR, and Di Chiro G. Mapping of brain tumor metabolites with proton MR spectroscopic imaging: clinical relevance. Radiology, 1992; 185: 675–686.
32. Usenius JP, Vainio P, Hernesniemi J, and Kauppinen RA. Choline-containing compounds in human astrocytomas studied by 1H NMR spectroscopy *in vivo* and *in vitro*. J. Neurochem. 1994; 63: 1538–1543.
33. Negendank WG, Brown TR, Evelhoch JL, Griffiths JR, Liotta LA, Margulis AR, Morrisett JD, Ross BD, and Shtern F. Proceedings of a National Cancer Institute workshop: MR spectroscopy and tumor cell biology. Radiology, 1992; 185: 875–883.
34. Leach MO, Verrill M, Glaholm J, Smith TA, Collins DJ, Payne GS, Sharp JC, Ronen SM, McCready VR, Powles TJ, and Smith IE. Measurements of human breast cancer using magnetic resonance spectroscopy: a review of clinical measurements and a report of localized 31P measurements of response to treatment. NMR Biomed. 1998; 11: 314–340.
35. Jordan BF, Black K, Robey IF, Runquist M, Powis G, and Gillies RJ. Metabolite changes in HT-29 xenograft tumors following HIF-1alpha inhibition with PX-478 as studied by MR spectroscopy *in vivo* and *ex vivo*. NMR Biomed. 2005; 18: 430–439.
36. Payne GS and Leach MO. Applications of magnetic resonance spectroscopy in radiotherapy treatment planning. Br. J. Radiol. 2006; 79: 16–26.
37. Shah N, Sattar A, Benanti M, Hollander S, and Cheuck L. Magnetic resonance spectroscopy as an imaging tool for cancer: a review of the literature. J. Am. Osteopath. Assoc. 2006; 106: 23–27.
38. Taper H, Woolley GW, Teller MN, Lardis MP. A new transplantable mouse liver tumor of spontaneous origin. Cancer Res. 1966; 26: 143–148.
39. Port M, Corot C, Raynal I, and Rousseaux O. Novel compositions magnetic particles covered with gem-bisphosphonate derivatives. US Patent 2004/0253181 A1.
40. Iannone A, Federico M, Tomasi A, Magin RL, Casasco A, Calligaro A, and Vannini V. Detection and quantification in rat tissues of the superparamagnetic magnetite resonance contrast agent dextran magnetite as demonstrated by electron spin resonance spectroscopy. Invest. Radiol. 1992; 27: 450–455.
41. Fujii H, Yoshikawa K, and Berliner LJ. *In vivo* fate of superparamagnetic iron oxides during sepsis. Magn. Reson. Imag. 2002; 20: 271–276.
42. Hamstra DA, Rehemtulla A, and Ross BD. Diffusion magnetic resonance imaging: a biomarker for treatment response in oncology. J. Clin. Oncol. 2007; 25: 4104–4109.
43. Padhani AR, Liu G, Mu-Koh D, Chenevert TL, Thoeny HC, Takahara T, Dzik-Jurasz A, Ross BD, Van Cauteren M, Collins D, Hammoud DA, Rustin GJS, Taouli B, and Choyke PL. Neoplasia, 2009; 11: 102–125.
44. Bizzi A, Movsas B, Tedeschi G, Phillips CL, Okunieff P, Alger JR, and Di Chiro G. Response of non-Hodgkin lymphoma to radiation therapy: early and long-term assessment with H-1 MR spectroscopic imaging. Radiology, 1995; 194: 271–276.
45. Schwarz AJ, Maisey NR, Collins DJ, Cunningham D, Huddart R, and Leach MO. Early *in vivo* detection of metabolic response: a pilot study of 1H MR spectroscopy in extracranial lymphoma and germ cell tumours. Br. J. Radiol. 2002; 75: 959–966.
46. Seierstad T, Røe K, Olsen DR. Noninvasive monitoring of radiation-induced treatment response using proton magnetic resonance spectroscopy and diffusion-weighted magnetic resonance imaging in a colorectal tumor model. Radiother. Oncol. 2007; 85: 187–194.
47. Strauss HW, Blankenberg F, Vanderheyden JL, and Tait J. Translational imaging: imaging of apoptosis. Handb. Exp. Pharmacol. 2008; 185: 259–275.
48. Beloueche-Babari M, Chung YL, Al-Saffar NM, Falck-Miniotis M, Leach MO. Metabolic assessment of the action of targeted cancer therapeutics using magnetic resonance spectroscopy. Br. J. Cancer. 2010; 102: 1–7.